Artificial neural network enabled accurate geometrical design and optimisation of thermoelectric generator

Yuxiao Zhu[a§], Daniel W. Newbrook[a§], Peng Dai[a], C. H. (Kees) de Groot[a] and Ruomeng Huang[a*]

[a]*School of Electronics and Computer Science, University of Southampton, Southampton, United Kingdom*

Abstract

The ever-increasing demand for renewable energy and zero carbon dioxide emission have been the driving force for the development of thermoelectric generators with better power generation performance. Alongside with the effort to discover thermoelectric materials with higher figure-of-merit, the geometrical and structural optimisation of thermoelectric generators are also essential for maximized power generation and efficiency. This work demonstrates for the first time the application of artificial neural network, a deep learning technique, in forward modelling the maximum power generation and efficiency of a thermoelectric generator and its application in the generator design and optimisation. After training using a dataset containing 5000 3-D finite element method based simulations, the artificial neural networks with 5 layers and 400 neurons per layer demonstrate extremely high prediction accuracy over 98% and are able to operate under both constant temperature difference and heat flux conditions while taking into account of the contact electrical resistance, surface heat transfer and other thermoelectric effects. Coupling with genetic algorithm, the trained artificial neural networks can optimise the leg height, leg width, fill factor and interconnect height of the thermoelectric generator for different operating and contact resistance conditions. With almost identical optimised values obtained, our neural networks can realise geometrical optimisation within 40 s for each operating condition, which is averagely over 1,000 times faster than the optimisation performed by finite element method. The up-front computational time for the neural network can be recovered when more than 2 optimisations are needed. The successful application of this data-driven approach in this work clearly represents a new and cost-effective avenue for conducting system level design and optimisation of thermoelectric generators and other energy harvesting technologies.

Keywords: thermoelectric generator, optimisation, artificial neural network, genetic algorithm

Nomenclature

TEG	Thermoelectric Generator	GA	Genetic Algorithm
ZT	Dimensionless figure of merit	ANN	Artificial Neural Network
Q_{in}/A	Heat flux density (mW/cm^2)	H_{TE}	Height of the TEG leg (mm)
T_h	Hot-side temperature (K)	H_{IC}	Height of the interconnect (mm)
T_c	Cold-side temperature (K)	W_n	Width of the n-type leg (mm)
R_C	Electrical contact resistance (Ω)	W_p	Width of the p-type leg (mm)
ρ_C	Contact resistivity (Ω·m^2)	A	Surface area (cm^2)

FF	Fill factor	PD_{max}	Power density (mW/cm^2)
σ	Electrical Conductivity (S/m)	η	Efficiency (%)
S	Seebeck coefficient (μV/K)	k	Thermal Conductivity (W/m·K)
$\vec{J}$	Current density vector (A/cm^2)	Π	Peltier Coefficient (J/C)
$\vec{q}$	Heat flux vector (mW/cm^2)	C_p	Heat Capacity (J/K)
$\vec{E}$	Electric field vector (V/m)	D	Density (kg/m^3)
$\vec{u}$	Velocity vector (m/s)		

1. Introduction

The global energy consumption has doubled over the past three decades with over 80% of the consumed energy supplied by conventional combustion energy (e.g. coal, natural gas, oil) [1,2]. Producing a secure, sustainable and efficient energy supply that meets the demands of increasing global population and reducing the environmental impact of CO_2 emissions are widely acknowledged to be among the most important societal challenges for the present generation [3]. Staying on the path to net-zero emission requires immediate and massive deployment of all clean and efficient energy technologies. As depicted in the net-zero emission by 2050 scenario (NZE), renewable energy conversion technologies play a central part in emission reduction across all sectors and are account for 90% of all electricity generation [2]. One significant energy source that can be recycled is the waste heat generated during the conventional fossil-fuel based power generation process. In fact, 60% of the fossil energy is wasted in the form of heat. Recovery of just 1% of the wasted energy would provide over 200 TWh of electricity annually (market value *ca.* $20 billion), and bring very significant associated benefits *via* reduction in CO_2 emission [4].

Thermoelectric generators (TEGs), which are capable of harvesting waste heat and converting this thermal energy into electricity, have the potential to contribute significantly to the energy supply by reducing the inefficiency of current methods and reducing the dependency on fossil fuels. Based on the Seebeck effect, TEGs are formed by connecting n-type semiconductor materials and p-type semiconductor materials electrically in series and thermally in parallel across a temperature gradient to allowing current flow between the two legs [5,6]. Compared to other energy harvesting technologies, TEGs offer a simple configuration, maintenance-free solid-state operation, and lifetime high reliability that often significantly exceed those of the devices they power [7]. Despite its great potential, the relatively low energy conversion efficiency has limited the usage of TEG to applications such as electricity generation in extreme environments, waste heat recovery from automobile and industrial sites, and off-grid power supply [8]. To overcome this limitation, material and geometrical design optimisation have been researched extensively as the two main approaches to improve the TE efficiency. Developing materials with better thermoelectric properties (evaluated by the figure-of-merit, ZT) has been the main driving force in the TE society over the past decade [9,10]. Several material engineering strategies such as carrier concentration optimisation, nanostructuring, and band engineering have been proposed and materialised in significantly improved ZT values [11,12]. Materials including SnSe [13,14], PbTe-SrTe [15], and mosaic crystals [16,17] have all been reported to have ZT larger than 2, showing encouraging prospects for the large scale application of TEGs. With high performing TE materials being developed, the vital task shifts to the adequate translation of such high material properties into the actual performance of the TEG [18]. Despite the

exceptionally high efficiency of *ca.* 12% reported on a bismuth telluride/skutterudite segmented module [19], the research on this aspect is still lagging. It is rather rare for any TEG to demonstrate high efficiency, even when superior TE materials are integrated [12]. The main reason is the fact that output power of a TEG relies not only on the performance of the TE materials, but also critically on the TEG design including its geometrical configuration, contact resistance and its coupling with heat source/sink as well as environmental working conditions, which demands a comprehensive and holistic consideration in TEG design and optimisation [18,20].

Considering such complexity in TEG design, dedicated optimisation methods are preferred over the conventional analytical approach to perform optimisation. A simplified conjugate-gradient method (SCGM) was proposed by Liu et al. to realize the parametric optimisation for both TEG power and efficiency [21]. The widely used Taguchi method was also adopted by Chen et al. in TEG system to find the optimum conditions for maximizing the performance [22]. He et al. introduced a Hill-climbing algorithm to achieve a maximum power output [23]. More recently, genetic algorithm (GA), a subset of evolutionary computation in artificial intelligence (AI), has also been extensively explored for the application in TEG design. GA is a derivative-free optimisation method which is an appealing option for solving optimisation problems. It uses stochastic and direct-search methods to find good approximate solutions to complex problems with little to no prior knowledge of the optimisation problem. Ge et al. employed a non-dominated sorting genetic algorithm (NSGA-II) to identify the best geometric ratio for a segmented TEG [24]. Chen et al. applied the multi-objective genetic algorithm (MOGA) to determine the optimum leg length and area of thermoelectric elements based on a constant volume [25]. A similar algorithm was adopted by the same group to maximise the power of a segmented skutterudite TEG under different temperatures [26].

However, the performance of any of these optimisation methods is critically dependent on the coupled TEG model to accurately and efficiently identify the power output of TEGs. This is particularly challenging considering the non-linear thermoelectric effects and the intricate inter-dependence of each design parameter [27,28]. In general, TEG models can be established through both theoretical and numerical approaches. Table 1 provides a list of reported works based on these two approaches. For example, an early theoretical model proposed by Min et al. [29] investigated the effect of thermoelement length on the module's coefficient of performance. Gou et al. [30] developed a theoretical system model for a low-temperature waste heat thermoelectric generator setup. Newbrook et al. [31] built a simplified theoretical model for performance optimisation of a thin film based TEG. Although these theoretical models enable quick estimation of the TEG performance, the accuracy is limited by their grossly simplified assumptions and difficulty to incorporate related thermoelectric effects (e.g. Thomson effect) [32]. Numerical model based simulation also prevail due to its superiority in solving differential equations and ease of use [23]. Suter el al. [33] implemented a heat transfer model coupling one-dimensional (1-D) conduction through the thermoelement legs to study a thermoelectric stack. Similar 1-D model was also adopted by Shen et al. [32] to analyse the TEG performance with temperature-dependence of TE materials considered. Zhu et al. also used a similar model to investigate and optimise the performance of a segmented TEG [34]. However, most of these self-programmed models are limited to 1-D and certain TEG structures. Three-dimensional (3-D) modelling techniques are available in commercial software (e.g. COMSOL and ANASYS) which enable simultaneous incorporation of all thermoelectric effects and can provide high prediction accuracy for TEG optimisation [35]. For example, a 3-D ANASYS TEG model was coupled with the MOGA in both works report by Chen et al. [25,26], demonstrating very good agreements with experimental results. Meng et al. [36] build up a TEG model in COMSOL as the direct problem solver to facilitate the multi-objective optimisation of a thermoelectric energy conversion-utilization system. Ge et al. applied a 3-D COMSOL model in their evolutionary algorithm based optimisation of a segmented TEG [24]. The simplified conjugate-gradient method proposed by Liu et al. [21] was also coupled with a COMSOL based TEG model. By allowing simultaneous coupling of nearly all related TE effects, these models have superior

reliability in calculating TEG power performance. Nevertheless, such high accuracy for 3-D models comes at a cost of high computational demand. For example, tens of thousands of 3-D simulations are normally required in GA to optimise the design of TEG [25]. Moreover, this optimisation is only limited to one operating condition (e.g. temperature difference or heat flux). When optimisations under various conditions are required to match different applications, the computational demand can be prohibitive for its wide adoption for TEG optimisation applications. Modelling method that combines both high prediction accuracy and fast speed is therefore key for TEG design and optimisation.

Table 1 List of a literature review of TEG forward modelling methods.

Forward modelling method	**TEG structure**	**Ref**
Theoretical model	Bulk	[29]
Theoretical model	Bulk	[30]
Theoretical model	Thin film	[31]
Numerical model (1-D)	Bulk	[32]
Numerical model (1-D)	Bulk	[23]
Numerical model (1-D)	Bulk (stack)	[33]
Numerical model (1-D)	Bulk (segmented)	[34]
Numerical model (3-D, ANSYS)	Bulk	[35]
Numerical model (3-D, ANSYS)	Bulk	[25]
Numerical model (3-D, ANSYS)	Bulk (segmented)	[26]
Numerical model (3-D, COMSOL)	Bulk (two-stage)	[36]
Numerical model (3-D, COMSOL)	Bulk (segmented)	[24]
Numerical model (3-D, COMSOL)	Bulk (two-stage)	[21]

Deep learning is a subset of machine learning technology with most of its models based on artificial neural networks (ANNs). It has received great attention world-wide for its efficiency in analysing a vast number of datasets and its revolutionary impact to the field of computer vision [37,38] and speech recognition [39]. Recently, deep learning has been proposed to replace the conventional intuition based design process in nano-photonics [40,41], providing accurate and efficient design of optical storages [42], metasurfaces [43,44], and nanostructured colour filters [45,46]. In the energy sector, deep learning has been extensively used to model the energy consumption to forecast the energy demand [47,48] and electricity consumption [49]. It has also found application in solid-state systems to discover and predict the performance of new materials due to its outstanding capability of finding optimal solution from enormous data with much lower demand on computational resources [50,51]. Several pioneering works have also been reported on using machine learning to facilitate research on thermoelectric materials [52,53]. The idea of this data-driven approach is to predict the results based on approximation without explicitly solving the question. This is particular useful to model systems that involve a large number of parameters with complicated relations where analytical approaches are not readily available. Before the ANNs can perform the intended forward modelling, a training process needs to take place in which a dataset is required. This dataset, which normally involves a large number of input and output relations, can be generated by either numerical simulation or experimental results. However, this is a one-time investment and no significant computation will be needed once the network is properly trained. Despite such advantages, the application of deep learning in the forward modelling of TEG has never been reported.

This work reports the first ever deep learning based forward modelling of TEG using fully-connected ANNs that demonstrates both high accuracy and efficiency. The novel neural network can be used to predict TEG performance under different operating conditions (i.e. constant temperature difference and constant heat flux)

without the need of prior knowledge to the thermoelectric device. After training using a dataset generated from 3-D TEG model based on COMSOL simulations that take into account of the non-linear thermoelectric effects, temperature-dependent thermoelectric material properties, electrical contact resistance, and heat transfer with the ambient environment, the ANN is able to learn the complex underlying relations in the dataset and perform predictions in an accurate and fast manner. In addition, the application of such ANN in TEG design optimisation is also presented for the first time by coupling it with genetic algorithm. When multiple optimisations under different operating conditions are required, our ANN-enabled optimisation demonstrates superior cost-effectiveness comparing against the conventional 3-D modelling enabled optimisation, suggesting a significant saving of computational time and energy.

2. Method

2.1. Physical model and boundary conditions

Fig. 1a illustrates the TEG model investigated in this work, which contains a pair of n-type and p-type semiconductors. The thermoelectric materials used in this work are $Bi_2Te_{2.7}Se_{0.3}$ for the n-type leg and $Bi_{0.5}Sb_{1.5}Te_3$ for the p-type leg. The interconnect and capping materials are copper and quartz glass, respectively. The detailed thermoelectric properties such as Seebeck coefficient (S), electrical and thermal conductivities (σ and k) and ZT values of both materials are adopted from past studies [54,55] and presented in Fig. 1b – 1e. The correlations of the material properties as a function of temperature are tabulated in Table S1 in the Supplementary Information.

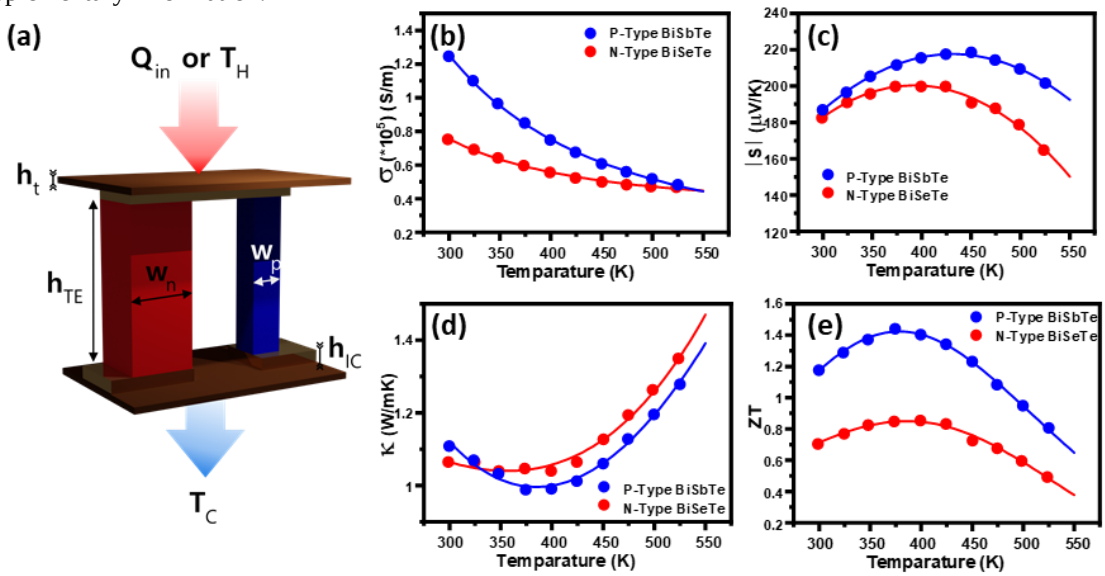

Fig.1. (a) Schematic of the singe-pair thermoelectric generator modelled in this study. Temperature dependent (b) Electrical conductivity, (c) Seebeck coefficient, (d) thermal conductivity and (e) ZT of the n-type and p-type semiconductors used for the thermoelectric generator. Data generated from [54,55].

The thermal boundary conditions are set to a constant cold-side temperature (T_C) of 300 K, and a convectional heat flux on all open internal surfaces with a heat transfer coefficient of 1 mW/(cm^2·K) and external temperature of 293.15 K to include surface heat convection to air [56]. For electrical boundary conditions, the TEG model is connected to an external load to form a circuit. The inlet and outlet of the metal substrate serve as a terminal (variable V) and the ground (V = 0 V) for the model.

The operating conditions are of paramount importance for TEG performance. Generally, TEGs can be operated under the condition of either constant temperature difference or constant heat flux. Both conditions are investigated separately in this work by applying a constant hot-side temperature (T_h) and constant heat flux density (Q_{in}/A). Electrical contact resistance (R_C) , a crucial factor for TEG [57], was included in the model by introducing a contact resistivity (ρ_C) between the thermoelectric material and the interconnect interfaces. The effect of varying geometrical parameters including the filling factor (FF), height of the TEG leg (H_{TE}), height of the interconnect (H_{IC}), and the widths of the n-type and p-type legs (W_n and W_p) on the TEG performance are investigated.

2.2. ANN dataset generation

Simulations based on the thermoelectric module in the COMSOL Multiphysics® software were used in this work to generate dataset for neural network training. This commercial simulation tool was chosen because of its high prediction accuracy and versatility in simulating different physical TEG models (e.g. segmented, asymmetrical). The simulated device is a single thermocouple shown in Fig. 1a. The details of the governing equations for this TEG model are provided in the Supplementary Information. Two datasets concerning the different operating conditions are generated separately. For each dataset, 5,000 random values were generated uniformly across the range for each parameter. The resolution of each parameter value is listed in Table 2. The distribution of each parameter is presented in Fig. S1 and Fig. S2 in the Supplementary Information.

Table 2 Ranges and resolutions of the geometrical parameters and operating conditions used in this work.

Geometrical Parameter	**Value Range**	**Resolution**
Height of the TE leg H_{TE}	0.5 – 5 mm	0.1 mm
Height of the interconnect H_{IC}	0.5 – 3 mm	0.1 mm
Filling factor FF	0.05 – 0.95	0.01
Width of the n-type TE leg W_n	0.5 – 5 mm	0.1 mm
Width of the p-type TE leg W_p	0.5 – 5 mm	0.1 mm
Working condition	**Value Range**	**Resolution**
Contact resistivity ρ_C	10^{-9} – 10^{-7} Ω·m^2	10^{-9} Ω·m^2
Input heat flux density Q_{in}/A	100 – 500 mW/cm^2	1 mW/cm^2
Hot-side temperature T_h	300 – 500 K	1 K

The obtained 5,000 parameter sets were subsequently simulated in COMSOL to obtain TEG power performance. Two performance factors, maximum output power density (PD_{max}) and efficiency (η), were extracted from the simulation. For each parameter set, the electrical terminal was connected directly to a load resistance and swept from 1/100 to 100 times the internal resistance. The maximum output power was then extracted from a parabolic fit of the output power against the current out as shown in Fig. S3. The efficiency was calculated as the percentage ratio between the maximum output power and the input heat power.

The impact of mesh sizes on the simulation accuracy was evaluated by simulating the same parameter set with difference meshs as shown in Fig. S4. The results showed that the maximum output power obtained from a “Finer” (6,824 elements) and “Extremely Finer” (60,236 elements) configurations are almost identical with 0.09% difference. Finer mesh configuration was therefore employed to simulate all parameter sets for

minimizing computational time while maintaing the accuracy. The ANN dataset generation was completed after the simulated TEG power performance were included. The distributions of the power performance in the two datasets can be found in Fig. S1 and Fig. S2.

2.3. ANN configuration and training

The configuration of the forward modelling network adopted in this work is shown in Fig. 2. The network was constructed by fully connecting the input layer of geometrical parameters (FF, H_{TE}, H_{IC}, W_n, W_p) and operating conditions (ρ_C, Q_{in}/A or T_h) with output layer of power performance (PD_{max} and η) through several hidden layers. Prior to training, a loss function must be established to allow back propagation. The loss function was defined as the mean squared error (MSE) between the predicted power performance and the true power performance (i.e. results from COMSOL simulation). In the training process, the datasets were divided into three sub-datasets for training (4,000), validation (500) and testing (500) purposes. The training data were fed to the ANN to optimise the network by updating the weights and bias of each neuron through back propagation; validation data were used to examine the network, serving as a check of the training and an indicator for any overfitting or under-fitting behavior during the training process; test data were completely new data to the network and were used to test the prediction accuracy of the network after training. All neural network algorithms were developed *via* the Python platform using the Pytorch module. Detailed information for the training process can be found in the Supplementary Information.

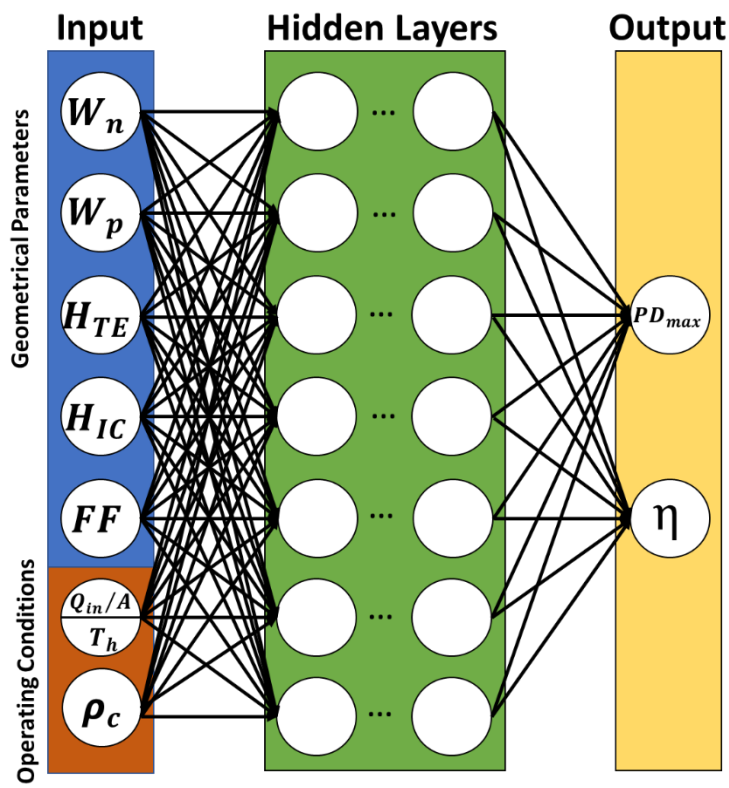

Fig.2. Architecture of the forward modelling neural network for predicting power performance of the TEG model. The input layer contains geometrical parameters (FF, H_{TE}, H_{IC}, W_n, W_p) and operating conditions (ρ_C, Q_{in}/A or T_h). The output layer contains power performance values (PD_{max} and η).

2.4. Genetic algorithm

Genetic algorithm (GA) was adopted in this work for geometrical parameter optimisation. Prior to the optimisation, the operation conditions (ρ_C, Q_{in}/A or T_h) can be freely selected to reflect the best matching practical scenarios. The optimisation flow chart is illustrated in Fig. 3. The optimisation is a refined iterative process in which an elite percentage of the geometrical parameter sets (FF, H_{TE}, H_{IC}, W_n, W_p) are retained through each iteration, allowing the samples to genetically evolve until the best option has been identified. A population size (i.e. candidate designs) of 100 was defined. Within each generation, 100 designs were firstly predicted by the ANN or COMSOL to obtain 100 power performance values. These values were compared with each other while the designs with highest power performances were selected into the next generation. Another 100 candidate designs were subsequently generated based on the best solution obtained in the previous generation with certain mutations and crossovers. In this way, the process is evolved gradually toward better solutions. Details about GA in this work can be found in Supplementary Information.

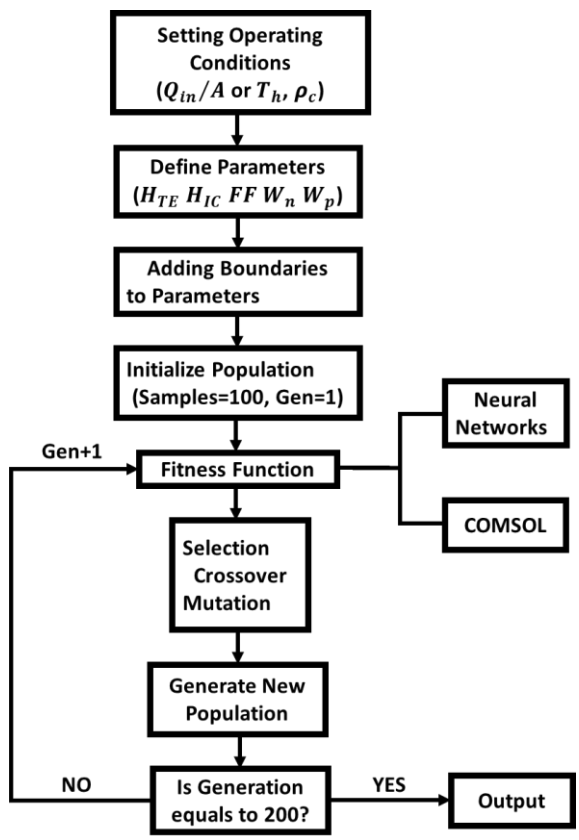

Fig.3. Optimisation flow chart of the genetic algorithm process. Both neural networks and COMSOL simulation have been used and compared for fitness function calculation.

3. Results and discussion

3.1. ANN performance under constant temperature difference (T_h)

We will first evaluate the prediction performance of ANN for TEG operating under constant temperature difference. The selection of the hyperparameters (i.e. number of hidden layers and neurons per layer) is crucial to the performance of the network. A systematic study was therefore conducted to investigate the impact of the hyperparameters for this ANN. Fig. 4a presents the validation loss curves over epochs for neural networks with the neuron numbers per layer ranging from 20 to 400 and fixed layer number of 5 (Detailed investigation of layer numbers can be found in Supplementary Information). The decrements of the loss curves against epochs indicate the reduction of MSEs through back propagation. No overfitting was observed for all training processes. After 2000 epochs, all MSEs are stabilized, signaling the completion of the training process. It can be observed that an increase of the neuron numbers from 20 to 400 leads to a lower MSE, suggesting the increasing complexity could be beneficial to the ANN performance. This needs to be confirmed by predicting the parameter sets in the test dataset which the networks have never seen before. Here we define the relative error between the ANN predicted and true power performance (i.e. performance obtained from COMSOL simulation) to compare the performance of the ANN. The relative error can be calculated as:

$$Relative\ error = \left|P_{true} - P_{predicted}\right| / P_{true} \tag{5}$$

where P_{true} is the power performance obtained from COMSOL simulation which include both power PD_{max} and η. $P_{predicted}$ is the power performance obtained from ANN. The distribution and average of the relative error as a function of layer numbers are plotted in Fig. 4b. It is evident that the average relative error in the test dataset decreases significantly from 0.044 to 0.019 as neurons per layer increases from 20 to 400. The prediction accuracy of the ANNs can then be calculated by

$$Prediction\ accuracy = (1 - relative\ error) \times 100\% \tag{6}$$

A relative error of 0.019 therefore indicates a very high prediction accuracy over 98%. The distribution of the relative error also suggests that a majority of the errors are within 3%, indicating an extremely high prediction accuracy of the network. Therefore, the network of 5 layers and 400 neurons per layer was adopted for this operating condition.

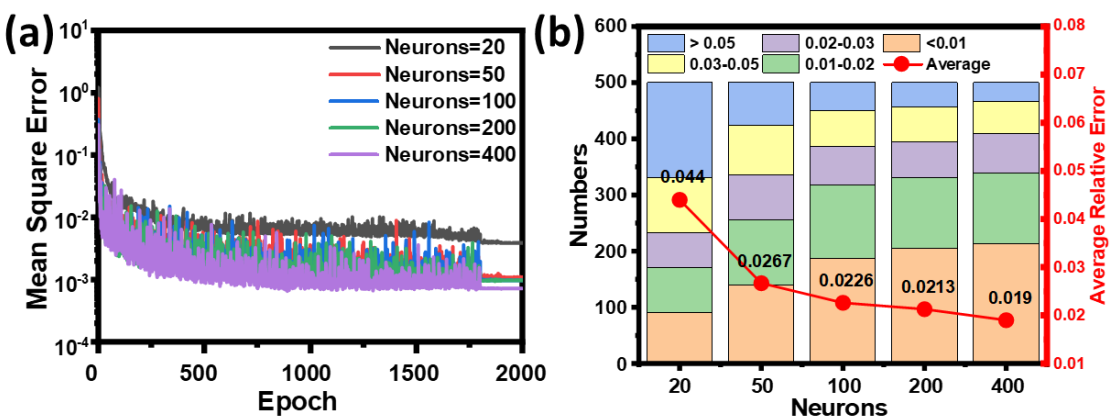

Fig.4. The neural network training for forward modelling TEG power performance under the operation condition of constant temperature difference. The (a) validation loss curves and (b) the histogram of the probability and average relative errors of the ANNs with different neurons per layer.

Fig. 5 plots the comparison between the true (simulated) power performance of PD_{max} and efficiency values in the test dataset with the ones predicted by the ANN. It can be clearly observed that the high prediction accuracy of our ANN prevails over three orders of magnitude, producing a high coefficient of determination value (R^2) of over 0.999 for both PD_{max} and efficiency. This outstanding prediction accuracy over a large range is particular useful for its application in TEG optimisation.

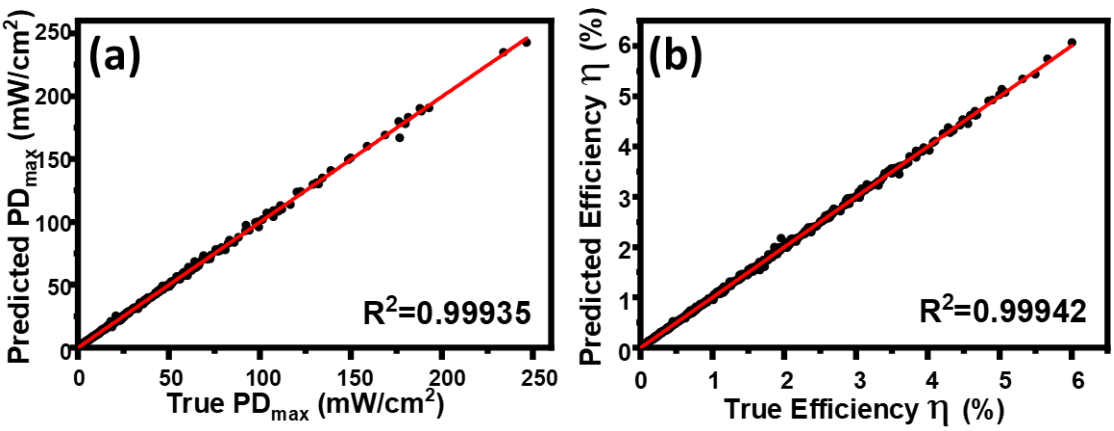

Fig.5. Scatter plot of the ANN predicted and the true (simulated) (a) PD_{max} and (b) efficiency η under the operating condition of constant temperature difference.

Once the forward TEG model is established, it can be used to investigate the impact of different parameters on the performance of TEG. As an example, the dashed lines in Fig. 6 presents the ANN predicted PD_{max} and η values as a function of H_{TE} and FF while the H_{IC}, W_n and W_p values were fixed at 1.5 mm, 2.5 mm and 2.5 mm, respectively. Under the operating condition of $T_h = 400\ K$ and $\rho_C = 10^{-8}\ \Omega \cdot m^2$, larger FF is favourable for achieving larger PD_{max} as shown in Fig.6a. In our model, changing of FF is achieved by varying the total area of the model to ensure the W_n amd W_p remain unchanged. A large FF implies a small TEG area which leads to reduced interconnect electrical resistance and increased PD_{max}. The dependence of H_{TE} is more complicated. Small H_{TE} limits the power performance with small temperature gradient over the TE legs, while large H_{TE} deteriorates the power by increasing the electrical resistance. This results in an optimised H_{TE} for each FF. On the other hand, the efficiency η undergoes different trends with varying H_{TE} and FF as shown in Fig.6b. Although a large FF is still advantageous, its benefit reduces at larger FF values due to the concurrently increased Q_{in}. Unlike PD_{max}, higher η can be achieved with larger H_{TE} values when FF is larger than 0.1. COMSOL simulations were also conducted for the same parameter sets (dots in Fig. 6) and achieved high consistency with the results generated by ANN as shown in Fig. 6. This suggests that our ANN can be used to investigate TEG power dependence on different parameters with high accuracy.

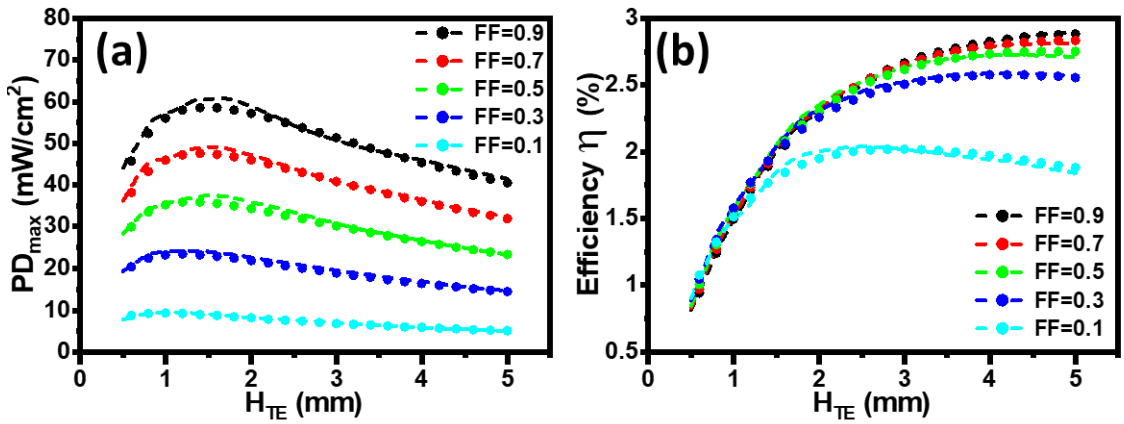

Fig.6. (a) PD_{max} and (b) efficiency η obtained from ANN (dashed lines) and COMSOL simulation (dots) as a function of H_{TE} and FF. The operating condition chosen is T_h of 400 K and ρ_C of 10^{-8} Ω·m^2. The H_{IC}, W_n and W_p values were fixed at 1.5 mm, 2.5 mm and 2.5 mm, respectively.

Once the network is trained and verified, it can be used for design optimisation. Two separate optimisations have been conducted to maximize power and efficiency respectively. In both cases, the operating condition of $T_h = 400\ K$ and $\rho_C = 10^{-8}\ \Omega \cdot m^2$, were chosen as an example. Fig. 7a and Fig.7b plot the GA convergence curves for power and efficiency optimisations, respectively. Both processes converge well after *ca.* 100 generations. A maximum power density of 70 mW/cm^2 was identified (Fig. 7a) while the maximum efficiency was found to be 3.2% (Fig. 7b). It is clear the designs (shown in the inset) reaching those two optimised values are significantly different.

To verify the effectiveness of our GA optimisation process, parameter sweeps of both H_{TE} and FF were conducted as shown in Fig. 7c to 7f. Under a constant T_h of 400 K, the optimised H_{TE} is 1.3 mm to achieve the largest PD_{max}. This is confirmed by sweeping its value from 0.5 mm to 5 mm and evaluating the performance of the TEG by ANN and simulation as shown in Fig. 7c. On the other hand, maximum efficiency η requires the optimised H_{TE} to reach the upper limit (5 mm) of the pre-set range (Fig. 7d). The discrepancy of the optimised H_{TE} values can be explained by the reducing Q_{in} as H_{TE} increases, leading to higher η but smaller PD_{max}. In both cases, results obtained from ANN (black lines) are highly consistent with that from simulation (blue dots). The optimisation of FF was also investigated. ANN coupled GA has found the largest FF (0.95) in the pre-set range for best PD_{max}. Increasing FF results in larger PD_{max} (shown in Fig. 7e), which is largely due to the reduction of the TEG electrical resistance. Similarly, a large FF is also required for high efficiency η (shown in Fig. 7f) as the PD_{max} increment from larger FF outweighs the increment of Q_{in}. Again, all results generated by ANN illustrate good matches with that from the simulation, further confirming the accuracy of our ANN.

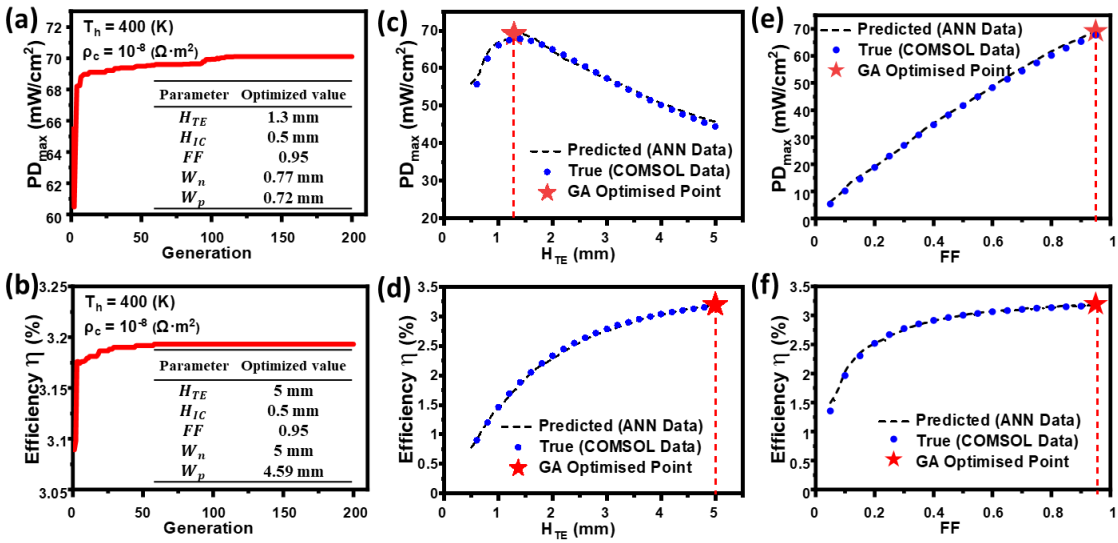

Fig.7. (a) Convergence curve of genetic algorithm for (a) PD_{max} and (b) η under an operating condition of T_h is 400 K and ρ_C is 10^{-8} Ω·m^2. Fig.12. Comparison of PD_{max} and efficiency η obtained from ANN (black line) and COMSOL simulation (blue dots) as a function of (c, d) H_{TE} and (e, f) FF. The optimised values are listed in the inset table and labelled by the red dots.

The key advantage of the deep learning aided approach is its extremely high design efficiency. Here we provide a direct comparison between the developed ANN and the COMSOL simulation by coupling both approaches with GA to execute the same optimisation tasks. Fig.8a and 8b present the optimised PD_{max} and efficiency η for different T_h conditions. Both optimised values increase with larger T_h. It is evident that all optimised values from the two approaches are almost identical with similar geometrical parameters obtained (listed in Table S3). However, the average time for COMSOL simulation coupled optimisation was 57,600 s (*ca.* 16 hrs) while it only took an average of 40 s for ANN to complete one optimisation. Although ANN requires a one-time investment for dataset generation (125,106 s, *ca.* 35 hrs) and network training (248 s), it is a much more cost-effective way if optimisations under multiple T_h conditions are required. Figure 8c plots the time required for both methods to perform multiple number of optimisations. It is clear that the amount of time saved by using ANN easily recovers the up-front computational time for the network when more than 2 optimisations are needed. Similarly, in Fig. 8d and 8e, optimisation against different ρ_C results in good agreements between the ANN and COMSOL simulation coupled optimisations. However, the former approach only requires an average of 35 s while the latter demands 40,000 s (*ca.* 11 hrs) for each optimisation. Significant time saving can be achieved if more than 3 optimisations are required as shown in Figure 8f. In both cases, improvement of computational efficiency of over 1,000 times were obtained. This superior design efficiency offered by ANN represents not only a significant saving of computational time but also computational energy.

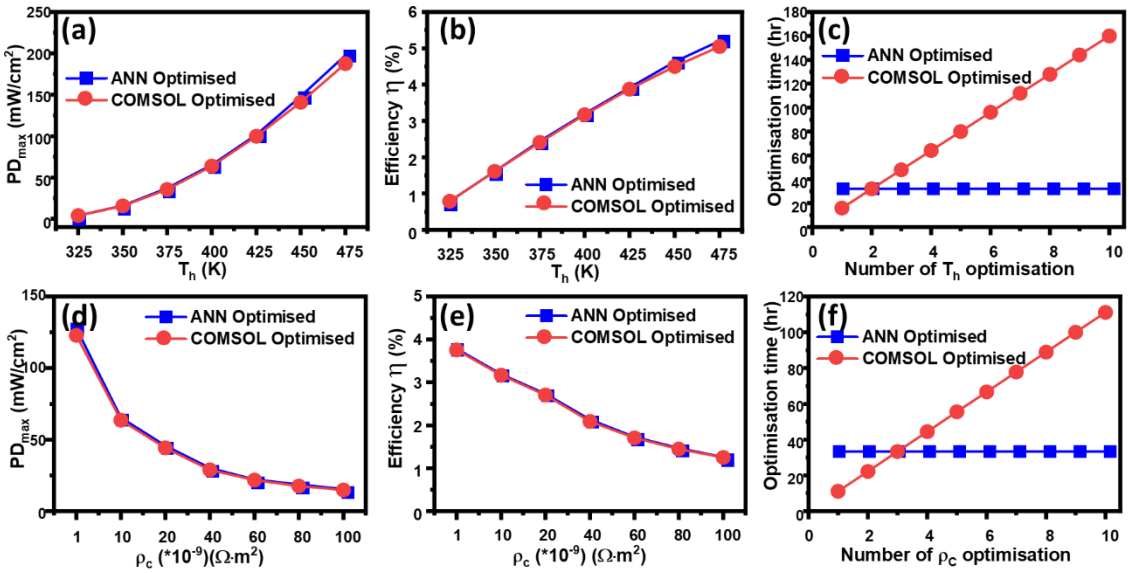

Fig.8. Optimisation of (a) PD_{max} and (b) efficiency η by GA coupled with ANN (blue dots) and COMSOL simulation (red dots) as a function of T_h, (c) required optimisation time of both methods for different T_h conditions; optimisation of (d) PD_{max} and (e) efficiency η by GA coupled with ANN and COMSOL as a function of ρ_C, (f) required optimisation time of both methods for different ρ_C conditions.

3.2. ANN performance under constant heat flux

We now turn our focus on the operating condition of constant heat flux. As the efficiency can be directly converted from power output, only PD_{max} will be presented and discussed in this section. The hyperparameter optimisation was also conducted by varying the neuron numbers per layer. As shown in Fig. 9a, the stabilized validation loss is smallest for network with most neurons per layer of 400. Similar to the previous condition, relative error was found to decrease from 0.0424 to 0.0177 with neurons per layer increasing from 20 to 400 as shown in Fig. 9b. This 5-layer and 400 neurons per layer network with a prediction accuracy over 98% was adopted for this condition.

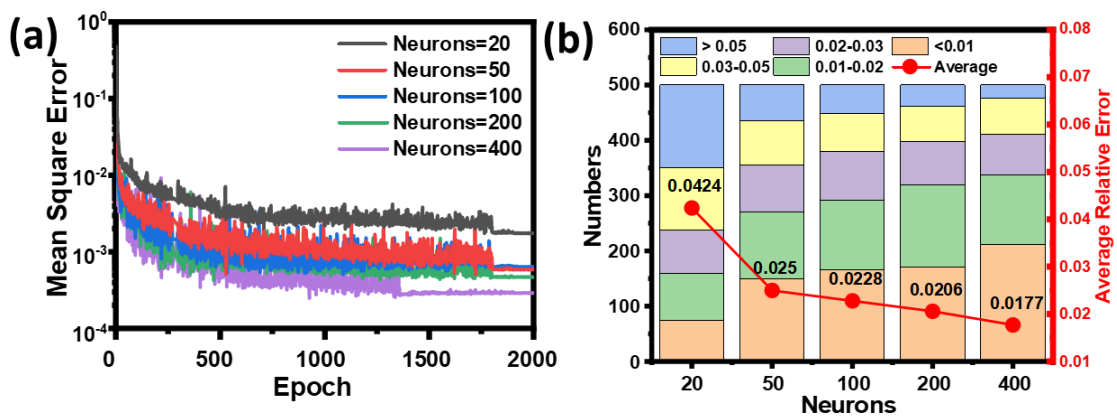

Fig.9. The neural network training for forward modelling TEG power performance. The (a) validation loss curves and (b) the histogram of the probability and average relative errors of the ANNs with different neurons per layer.

Fig. 10 compares the maximum power output PD_{max} from the ANN with the true (COMSOL simulated) values in the test dataset. Again, high consistency can be observed between the true values and the ANN predicted values with a high coefficient of determination value (R^2) of 0.99943, showing great prediction accuracy over the entire power range.

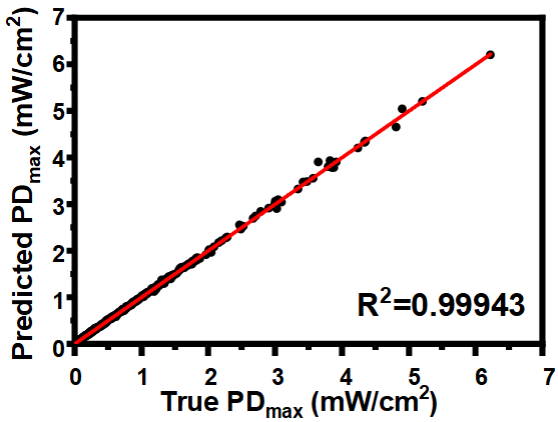

Fig.10. Scatter plot of the ANN predicted and the true (simulated) maximum power density under the operating condition of constant heat flux.

The analytical study under the constant heat flux condition were also conducted using this network to investigate the impact of H_{TE} and FF. As an example, the operating condition was chosen to be $Q_{in}/A = 300\ mW/cm^2$ and $\rho_C = 10^{-8}\ \Omega \cdot m^2$ while the H_{IC}, W_n and W_p values were fixed at 1.5 mm, 2.5 mm and 2.5 mm, respectively. Fig. 11 presents the PD_{max} as a function of H_{TE} and FF. It is clear that PD_{max} increases with increasing leg length due to larger temperature gradient created, implying an increase in η as well. However, the rate of increment decreases at higher H_{TE} values due to the adverse impact of larger electrical resistance. On the other hand, smaller FF is preferred to achieve high power performance. A smaller FF implies a larger TEG area which leads to a larger temperature difference and PD_{max}. In all cases, the simulation results (dots in Figure 11) show high consistence with the results generated by ANN (dashed lines in Figure 11).

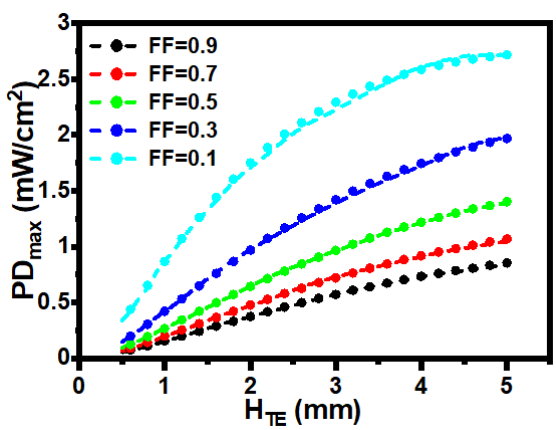

Fig.11. PD_{max} obtained from ANN (dashed lines) and COMSOL simulation (dots) as a function of H_{TE} and FF. The operating condition chosen is Q_{in}/A of 300 mW/cm^2 and ρ_C of 10^{-8} Ω·m^2. The H_{IC}, W_n and W_p values were fixed at 1.5 mm, 2.5 mm and 2.5 mm, respectively.

.

After establishing the prediction accuracy of our network, we will now evaluate the application of the ANN in TEG optimisation by coupling it with GA. Similar operating condition of $Q_{in}/A = 300\ mW/cm^2$ and $\rho_C = 10^{-8}\ \Omega \cdot m^2$ were chosen as an example for optimisation. Fig. 12a shows the convergence curve of GA for PD_{max} which converges after 50 generations. The optimised geometrical parameters are listed in the inset table. Sweepings of H_{TE} and FF were subsequently performed to verify the optimised values. Fig. 12b displays the sweep of H_{TE}. A shorter leg could lead to a beneficially smaller electrical resistance but also an adversely decreased temperature difference under this operating condition. It can be observed that the optimised value of 4.81 mm has been correctly identified by our GA. The sweeping of FF is plotted in Fig. 12c. A large FF implies a smaller TEG area which leads to a smaller temperature difference and maximum power output. On the other hand, a very small FF could induce large interconnect resistance that also deteriorates the power. An optimised FF of 0.11 was identified and was also verified by sweeping using both ANN and simulation. In addition, COMSOL simulations were also conducted using the same parameter sets. The simulated results (dots) show great match with the predicted results from ANN (line), further confirming the high accuracy of our network.

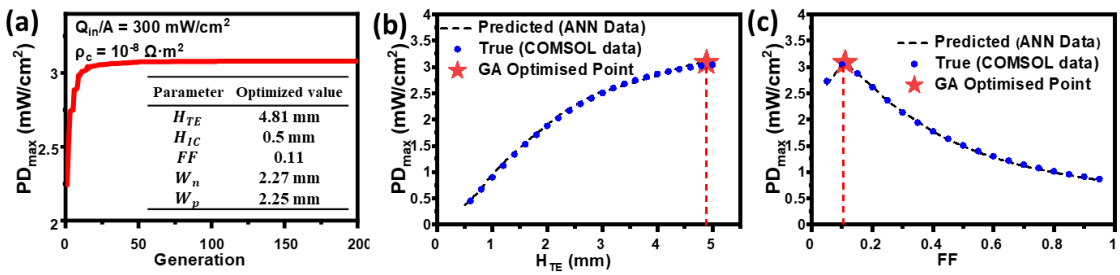

Fig.12. (a) Convergence curve of genetic algorithm for maximum power output under an operating condition of Q_{in}/A is 300 mW/cm^2 and ρ_C is 10^{-8} Ω·m^2. Comparison of PD_{max} obtained from ANN (black line) and COMSOL simulation (blue dots) as a function of (b) H_{TE} and (c) FF. The optimised values are listed in the inset table and labelled by the red dots.

Efficiency comparison between the developed ANN and the conventional simulation was also conducted under the constant heat flux condition. Fig.13a and 13b present the optimised PD_{max} under different Q_{in}/A and ρ_C values. As expected, larger Q_{in}/A and smaller ρ_C can produce larger optimised PD_{max}. Highly consistent optimised values were obtained from the ANN and COMSOL simulation approaches (detailed list of optimised parameters can be found in Supplementary Information). The average optimisation time for ANN coupled GA is 40 s while is 60,000 s (*ca.* 16 hrs) for COMSOL coupled GA, representing a saving of computational time and resources over 1,000 times. This indicates significant time-savings when more than 2 optimisations are required (shown in Fig.13c).

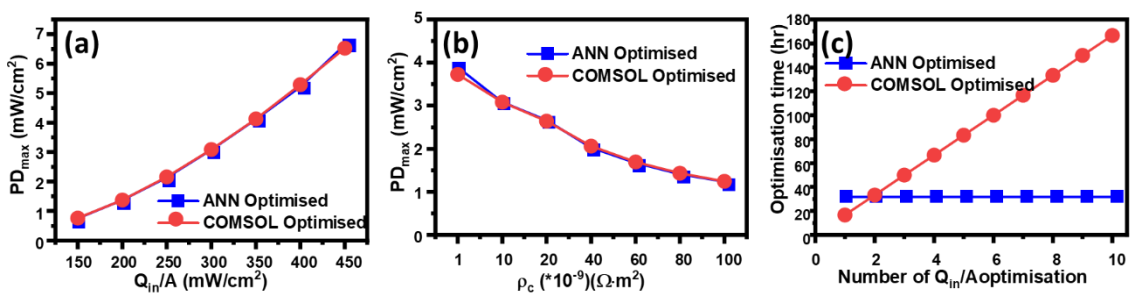

Fig.13 PD_{max} optimised by GA coupled with ANN (blue dots) and COMSOL simulation (red dots) as a function of (a) Q_{in}/A and (b) ρ_C; (c) required optimisation time of both methods for different number of Q_{in}/A conditions.

The successful implementation of ANN for TEG power performance prediction in this work has certainly suggested ANN as a powerful tool to assist future investigation and design of thermoelectric related devices. One main advantage of this technology is the needlessness of any prior knowledge to the device as the ANN will "learn" from the dataset. The quality of the dataset is therefore key to the ANN performance. In this work, 3-D COMSOL simulation was used to generate the dataset as it takes into account most of the non-linear thermoelectric effects which are normally ignored in other modelling methods due to complexity. This provided simulation results that were close to real devices. Once trained using a dataset with limited number of parameter-performance relations, this ANN can "learn" the "knowledge" and generate unlimited performance predictions with high accuracy. This is beneficial for analysing the relations between each parameter and the TEG performance. Although this work used a conventional TEG model as a demonstration, the ANN can be applied to investigate more complicated TEG structures (e.g. segmented, asymmetrical and multi-stage) as well as hybrid devices such as solar-TEG where parameter-performance relations are not available. It is also worth pointing out the limitation of our network. Even though our ANN has proved to be cost-effective in design when multiple optimisations are required, the up-front investment on computational resource is still high (i.e. *ca.* 35 hrs in this work). This is mainly due to the time needed to generate the dataset using COMSOL. It can be observed from Fig. S1h-I and Fig. S2h-i that the outputs of the dataset (i.e. TEG power performance) are not uniformly distributed as the inputs. In particular, number of outputs at high and low ends are much less than those in the middle due to the non-linear relation between the inputs and outputs. A relatively large dataset (i.e. 5,000 in this work) is necessary to ensure high prediction accuracy over the entire TEG performance range (shown in Fig. 5 and Fig. 10). Further improvements in both the network design and training process are required to reduce the need for such large dataset.

4. Conclusions

The application of the artificial neural network, a deep learning technique, in forward modelling of the power performance of a thermoelectric generator has been demonstrated for the first time. After training using a dataset from 3-D COMSOL simulations, the neural networks demonstrate extremely high prediction accuracy over 98% and are able to operate under both constant temperature difference and heat flux conditions while taking into account the electrical contact resistance, surface heat transfer and other thermoelectric effects. It can be used to replace the conventional theoretical and numerical modelling methods to predict and analyse the thermoelectric generator performance without the need of prior knowledge. Analytical studies using the developed networks have been successfully conducted to investigate the impact of different parameters to the power performance, and the results have shown high consistency with the those generated from COMSOL simulation. This method is also shown to be extremely efficient and cost-effective in TEG design optimisation when coupling with genetic algorithm. With almost identical optimised values obtained, our neural networks demonstrate superior optimisation efficiencies that are averagely over 1,000 times better than the COMSOL simulation coupled optimisation. The successful application of artificial neural networks reported here clearly points towards the capability of deep learning approach to be applied in modelling and optimisation of thermoelectric generators with different structures as well as energy harvesting technologies for other renewable energy sources such as solar and wind..

Declaration of Competing Interest

The authors declare that they have no known competing financial interests or personal relationships that could have appeared to influence the work reported in this paper.

Acknowledgements

This work was supported by the UK STFC project (ST/P00007X/1) and EPSRC ADEPT project (EP/N035437/1). The authors acknowledge the use of the IRIDIS High Performance Computing Facility, and associated support services at the University of Southampton, in the completion of this work. DWN would like to thank both BAE and EPSRC for funding the iCASE studentship (EP/R512096/1). All data supporting this study are openly available from the University of Southampton repository at DOI: https://doi.org/10.5258/SOTON/D1903.

Appendix A. Supplementary Information

Supplementary Information is available.

References

[1] Aydin G. Production modeling in the oil and natural gas industry: An application of trend analysis. Pet Sci Technol 2014;32:555–64. https://doi.org/10.1080/10916466.2013.825271.

[2] IEA. Net Zero by 2050 - A roadmap for the global energy sector 2021:222.

[3] Freer R, Powell A V. Realising the potential of thermoelectric technology: A Roadmap. J Mater Chem C 2020;8:441–63. https://doi.org/10.1039/c9tc05710b.

[4] IEA report - Energy Prices. IEA 2020. https://doi.org/https://www.iea.org/reports/energy-prices-2020.

[5] Snyder GJ, Toberer ES. Complex thermoelectric materials. Nat Mater 2008;7:105–14. https://doi.org/10.1038/nmat2090.

[6] Tritt TM. Thermoelectric phenomena, materials, and applications. Annu Rev Mater Res 2011;41:433–48. https://doi.org/10.1146/annurev-matsci-062910-100453.

[7] Zhang QH, Huang XY, Bai SQ, Shi X, Uher C, Chen LD. Thermoelectric devices for power generation: Recent progress and future challenges. Adv Eng Mater 2016;18:194–213. https://doi.org/10.1002/adem.201500333.

[8] Champier D. Thermoelectric generators: A review of applications. Energy Convers Manag 2017;140:167–81. https://doi.org/10.1016/j.enconman.2017.02.070.

[9] Cai B, Hu H, Zhuang H-L, Li J-F. Promising materials for thermoelectric applications. J Alloys Compd 2019;806:471–86. https://doi.org/10.1016/j.jallcom.2019.07.147.

[10] Zhou X, Yan Y, Lu X, Zhu H, Han X, Chen G, et al. Routes for high-performance thermoelectric materials. Mater Today 2018;21:974–88. https://doi.org/10.1016/j.mattod.2018.03.039.

[11] Neophytou N, Foster S, Vargiamidis V, Pennelli G, Narducci D. Nanostructured potential well/barrier engineering for realizing unprecedentedly large thermoelectric power factors. Mater Today Phys 2019;11:100159. https://doi.org/10.1016/j.mtphys.2019.100159.

[12] Yang L, Chen ZG, Dargusch MS, Zou J. High Performance thermoelectric materials: Progress and their applications. Adv Energy Mater 2018;8:1–28. https://doi.org/10.1002/aenm.201701797.

[13] Zhao L-D, Lo S-H, Zhang Y, Sun H, Tan G, Uher C, et al. Ultralow thermal conductivity and high thermoelectric figure of merit in SnSe crystals. Nature 2014;508:373–7. https://doi.org/10.1038/nature13184.

[14] Duong AT, Nguyen VQ, Duvjir G, Duong VT, Kwon S, Song JY, et al. Achieving ZT=2.2 with Bi-doped n-type SnSe single crystals. Nat Commun 2016;7:1–6. https://doi.org/10.1038/ncomms13713.

[15] Tan G, Shi F, Hao S, Zhao L-D, Chi H, Zhang X, et al. Non-equilibrium processing leads to record high thermoelectric figure of merit in PbTe–SrTe. Nat Commun 2016;7:12167. https://doi.org/10.1038/ncomms12167.

[16] He Y, Lu P, Shi X, Xu F, Zhang T, Snyder GJ, et al. Ultrahigh thermoelectric performance in mosaic crystals. Adv Mater 2015;27:3639–44. https://doi.org/10.1002/adma.201501030.

[17] Zhao K, Qiu P, Song Q, Blichfeld AB, Eikeland E, Ren D, et al. Ultrahigh thermoelectric performance in $Cu_{2-y}Se_{0.5}S_{0.5}$ liquid-like materials. Mater Today Phys 2017;1:14–23. https://doi.org/10.1016/j.mtphys.2017.04.003.

[18] He R, Schierning G, Nielsch K. Thermoelectric devices: A review of devices, architectures, and contact optimization. Adv Mater Technol 2018;3:1700256. https://doi.org/10.1002/admt.201700256.

[19] Zhang Q, Liao J, Tang Y, Gu M, Ming C, Qiu P, et al. Realizing a thermoelectric conversion efficiency of 12% in bismuth telluride/skutterudite segmented modules through full-parameter optimization and energy-loss minimized integration. Energy Environ Sci 2017;10:956–63. https://doi.org/10.1039/c7ee00447h.

[20] Shittu S, Li G, Zhao X, Ma X. Review of thermoelectric geometry and structure optimization for performance enhancement. Appl Energy 2020;268. https://doi.org/10.1016/j.apenergy.2020.115075.

[21] Liu Z, Zhu S, Ge Y, Shan F, Zeng L, Liu W. Geometry optimization of two-stage thermoelectric generators using simplified conjugate-gradient method. Appl Energy 2017;190:540–52. https://doi.org/10.1016/j.apenergy.2017.01.002.

[22] Chen WH, Huang SR, Lin YL. Performance analysis and optimum operation of a thermoelectric generator by Taguchi method. Appl Energy 2015;158:44–54. https://doi.org/10.1016/j.apenergy.2015.08.025.

[23] He H, Wu Y, Liu W, Rong M, Fang Z, Tang X. Comprehensive modeling for geometric optimization of a thermoelectric generator module. Energy Convers Manag 2019;183:645–59. https://doi.org/10.1016/j.enconman.2018.12.087.

[24] Ge Y, Liu Z, Sun H, Liu W. Optimal design of a segmented thermoelectric generator based on three-dimensional numerical simulation and multi-objective genetic algorithm. Energy 2018;147:1060–9. https://doi.org/10.1016/j.energy.2018.01.099.

[25] Chen WH, Wu PH, Lin YL. Performance optimization of thermoelectric generators designed by multi-objective genetic algorithm. Appl Energy 2018;209:211–23. https://doi.org/10.1016/j.apenergy.2017.10.094.

[26] Chen WH, Chiou Y Bin. Geometry design for maximizing output power of segmented skutterudite thermoelectric generator by evolutionary computation. Appl Energy 2020;274:115296. https://doi.org/10.1016/j.apenergy.2020.115296.

[27] Wang J, Wang F, Yin L, Sendeku MG, Zhang Y, Cheng R, et al. A unipolar nonvolatile resistive switching behavior in a layered transition metal oxide. Nanoscale 2019;11:20497–506. https://doi.org/10.1039/c9nr07456b.

[28] Chen WH, Lin YX, Wang XD, Lin YL. A comprehensive analysis of the performance of thermoelectric generators with constant and variable properties. Appl Energy 2019;241:11–24. https://doi.org/10.1016/j.apenergy.2019.02.083.

[29] Min G, Rowe DM. Improved model for calculating the coefficient of performance of a Peltier module. Energy Convers Manag 2000;41:163–71. https://doi.org/10.1016/S0196-8904(99)00102-8.

[30] Gou X, Xiao H, Yang S. Modeling, experimental study and optimization on low-temperature waste heat thermoelectric generator system. Appl Energy 2010;87:3131–6. https://doi.org/10.1016/j.apenergy.2010.02.013.

[31] Newbrook DW, Huang R, Richards SP, Sharma S, Reid G, Hector AL, et al. Mathematical model and optimization of a thin-film thermoelectric generator. J Phys Energy 2019;2:014001. https://doi.org/10.1088/2515-7655/ab4242.

[32] Shen ZG, Wu SY, Xiao L, Yin G. Theoretical modeling of thermoelectric generator with particular emphasis on the effect of side surface heat transfer. Energy 2016;95:367–79. https://doi.org/10.1016/j.energy.2015.12.005.

[33] Suter C, Jovanovic ZR, Steinfeld A. A 1kWe thermoelectric stack for geothermal power generation - Modeling and geometrical optimization. Appl Energy 2012;99:379–85. https://doi.org/10.1016/j.apenergy.2012.05.033.

[34] Zhu L, Li H, Chen S, Tian X, Kang X, Jiang X, et al. Optimization analysis of a segmented thermoelectric generator based on genetic algorithm. Renew Energy 2020;156:710–8. https://doi.org/10.1016/j.renene.2020.04.120.

[35] Chen WH, Lin YX, Wang XD, Lin YL. A comprehensive analysis of the performance of thermoelectric generators with constant and variable properties. Appl Energy 2019;241:11–24. https://doi.org/10.1016/j.apenergy.2019.02.083.

[36] Meng JH, Wu HC, Wang L, Lu G, Zhang K, Yan WM. Thermal management of a flexible controlled thermoelectric energy conversion-utilization system using a multi-objective optimization. Appl Therm Eng 2020;179:115721. https://doi.org/10.1016/j.applthermaleng.2020.115721.

[37] Najafabadi MM, Villanustre F, Khoshgoftaar TM, Seliya N, Wald R, Muharemagic E. Deep learning applications and

challenges in big data analytics. J Big Data 2015;2:1–21. https://doi.org/10.1186/s40537-014-0007-7.

[38] Voulodimos A, Doulamis N, Doulamis A, Protopapadakis E. Deep learning for computer vision: A brief review. Comput Intell Neurosci 2018;2018. https://doi.org/10.1155/2018/7068349.

[39] Nassif AB, Shahin I, Attili I, Azzeh M, Shaalan K. Speech recognition using deep neural networks: A systematic review. IEEE Access 2019;7:19143–65. https://doi.org/10.1109/ACCESS.2019.2896880.

[40] So S, Badloe T, Noh J, Bravo-Abad J, Rho J. Deep learning enabled inverse design in nanophotonics. Nanophotonics 2020;9:1041–57. https://doi.org/10.1515/nanoph-2019-0474.

[41] Wiecha P, Arbouet A, Girard C, Muskens O. Deep learning in nano-photonics: inverse design and beyond. Photonics Res 2021:1–18. https://doi.org/10.1364/PRJ.415960.

[42] Wiecha PR, Lecestre A, Mallet N, Larrieu G. Pushing the limits of optical information storage using deep learning. Nat Nanotechnol 2019;14:237–44. https://doi.org/10.1038/s41565-018-0346-1.

[43] Ma W, Cheng F, Liu Y. Deep-learning-enabled on-demand design of Chiral metamaterials. ACS Nano 2018;12:6326–34. https://doi.org/10.1021/acsnano.8b03569.

[44] Xu L, Rahmani M, Ma Y, Smirnova DA, Kamali KZ, Deng F, et al. Enhanced light–matter interactions in dielectric nanostructures via machine-learning approach. Adv Photonics 2020;2:1. https://doi.org/10.1117/1.AP.2.2.026003.

[45] Gao L, Li X, Liu D, Wang L, Yu Z. A bidirectional deep neural network for accurate silicon color design. Adv Mater 2019;31:1905467. https://doi.org/10.1002/adma.201905467.

[46] Dai P, Wang Y, Hu Y, de Groot C, Muskens O, Duan H, et al. Accurate inverse design of Fabry–Pérot-Cavity-based color filters far beyond sRGB via a bidirectional artificial neural network. Photonics Res 2021;9:236–46. https://doi.org/10.1364/prj.415141.

[47] Aydin G, Jang H, Topal E. Energy consumption modeling using artificial neural networks: The case of the world's highest consumers. Energy Sources, Part B Econ Plan Policy 2016;11:212–9. https://doi.org/10.1080/15567249.2015.1075086.

[48] García-Martín E, Rodrigues CF, Riley G, Grahn H. Estimation of energy consumption in machine learning. J Parallel Distrib Comput 2019;134:75–88. https://doi.org/10.1016/j.jpdc.2019.07.007.

[49] Oğcu G, Demirel OF, Zaim S. Forecasting Electricity Consumption with Neural Networks and Support Vector Regression. Procedia - Soc Behav Sci 2012;58:1576–85. https://doi.org/10.1016/j.sbspro.2012.09.1144.

[50] Schmidt J, Marques MRG, Botti S, Marques MAL. Recent advances and applications of machine learning in solid-state materials science. Npj Comput Mater 2019;5. https://doi.org/10.1038/s41524-019-0221-0.

[51] Liu Y, Zhao T, Ju W, Shi S, Shi S, Shi S. Materials discovery and design using machine learning. J Mater 2017;3:159–77. https://doi.org/10.1016/j.jmat.2017.08.002.

[52] Wang T, Zhang C, Snoussi H, Zhang G. Machine learning approaches for thermoelectric materials research. Adv Funct Mater 2020;30:1–14. https://doi.org/10.1002/adfm.201906041.

[53] Wang ZL, Yokoyama Y, Onda T, Adachi Y, Chen ZC. Improved thermoelectric properties of hot-extruded Bi–Te–Se bulk materials with Cu doping and property predictions via machine learning. Adv Electron Mater 2019;5. https://doi.org/10.1002/aelm.201900079.

[54] Yan X, Poudel B, Ma Y, Liu WS, Joshi G, Wang H, et al. Experimental studies on anisotropic thermoelectric properties and structures of n-type Bi2Te2.7Se0.3. Nano Lett 2010;10:3373–8. https://doi.org/10.1021/nl101156v.

[55] Poudel B, Hao Q, Ma Y, Lan Y, Minnich A, Yu B, et al. High-thermoelectric performance of nanostructured bismuth antimony telluride bulk alloys. Science (80-) 2008;320:634–8. https://doi.org/10.1126/science.1156446.

[56] Kosky P, Balmer R, Keat W, Wise G. Mechanical Engineering. Explor. Eng., Elsevier; 2013, p. 259–81. https://doi.org/10.1016/B978-0-12-415891-7.00012-1.

[57] Bjørk R. The Universal Influence of Contact Resistance on the Efficiency of a Thermoelectric Generator. J Electron Mater 2015;44:2869–76. https://doi.org/10.1007/s11664-015-3731-7.